VIETNAM ACADEMY OF SCIENCE AND TECHNOLOGY

Vietnam Journal of MECHANICS

Volume 35 Number 1

ISSN 0866-7136

VN INDEX 12.666

1

2013

35th Anniversary

Vietnam Journal of Mechanics, VAST, Vol. 35, No. 1 (2013), pp. 67 – 77

FATIGUE PERFORMANCE OF TUBULAR X-JOINTS: NUMERICAL INVESTIGATION

Nguyen Chien Thang[1], **Qian Xudong**[2], **Ton That Hoang Lan**[3]
[1] *Duy Tan University, Da Nang, Vietnam*
[2] *National University of Singapore*
[3] *University of Architecture, Ho Chi Minh City, Vietnam*

Abstract. The cyclic actions due to waves, currents and winds on offshore platforms frequently cause fatigue cracks at hot-spot locations. The remaining fatigue life of such connections depends significantly on the fatigue driving force often measured by the stress-intensity factors. This study examines the fatigue performance of tubular joints fabricated using a new type of enhanced partial joint penetration weld details under constant-amplitude brace in-plane bending actions. The numerical study ascertains the crack propagation angle, the crack-front profile and the interaction between adjacent cracks on the stress-intensity factors.

Keywords: Fatigue, tubular X-joints, crack propagation, SIF, finite element model.

1. INTRODUCTION

Fatigue failure caused by the initiation and propagation of surface cracks near the hot-spot weld-toe locations imposes a critical threat to the safety of offshore structures and onshore bridges experiencing cyclic actions throughout their operational lives. The fabrication of welded components in these structures should therefore entail a convenient profile with high quality controls, which satisfy the fatigue requirement prescribed in design codes [1]. The complete joint penetration (CJP) welds, widely implemented in offshore jacket structures, require highly skilled workmanship in delivering quality welds meeting the code requirement [1]. The potential defects near the open root of the CJP welds may lead to detrimental failures of the platform under fatigue loads [2]. Qian *et al.* [2] proposed a new type of welding details, namely the enhanced partial joint penetration (PJP+) welds, which include a part of the member wall thickness as the inherent backing plate for the welding material. The enhanced partial joint penetration welds anticipate a controlled weld profile and inconsequential unfused weld root at the limit of API RP 2X [3] level C non-destructive test (NDT) requirement or equivalently the class X NDT requirement in AWS [1]. The understanding on the fatigue performance of this new set of weld details requires experimental efforts and numerical verifications to support their applications in realistic engineering projects.

The existing S-N curves for tubular connections [1, 4, 5], developed through experimental data accumulated over decades of research efforts [6-12], estimate the fatigue life of tubular joints with CJP welds corresponding to the through-thickness propagation of weld toe cracks at hot-spot locations. Qian *et al.* [2] showed, through a detailed finite element investigation, that the stress concentration factors (SCF) near the weld toe of the enhanced partial joint penetration welds in a tubular joint are similar to those computed near the toe of the complete joint penetration welds of the same tubular joint. The similar hot-spot stress ranges imply that the fatigue lives for tubular joints fabricated using these two types of weld details remain comparable if weld toe cracking dominates the fatigue failure. A review on the root severity for tubular joints using CJP welds [13] reveals that the stress concentration factors near the weld root remain relatively lower than those near the weld toe, with the maximum root SCF equal to about 80% of the maximum toe SCF in certain joint geometries.

This study aims to examine the fatigue behavior of two large-scale circular hollow section (CHS) X-joints fabricated using the enhanced partial joint penetration welds tested under constant amplitude loads, covering the initiation and propagation of weld toe cracks and the effect of weld grinding. The investigation highlights a few important aspects in the numerical procedure to estimate the stress-intensity factors (SIFs) and to predict the fatigue crack propagation life.

2. EXPERIMENTAL RESULTS

2.1. Experimental set-up

The two CHS X-joint specimens reported in the current study share the same global configuration and dimensions, as illustrated in Fig. 1. The main member (chord) of the

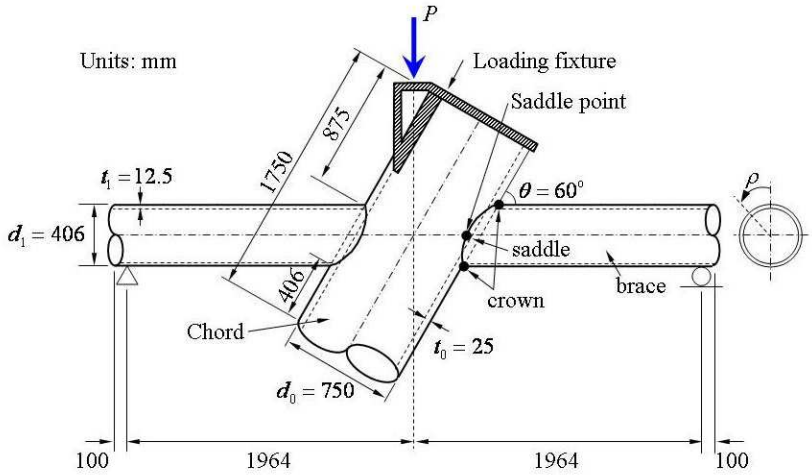

Fig. 1. Geometric configuration of the circular hollow section X-joint fabricated from the enhanced partial joint penetration welds

X-joint has an outer diameter (d_0) of 750 mm, with the wall thickness (t_0) equal to 25 mm. The secondary member (brace), which is profiled and welded to the chord, has an outer diameter (d_1) of 406 mm and a wall thickness (t_1) of 12.5 mm. The centerlines of the brace and the chord intersect at an angle of $\theta = 60^\circ$. Both specimens have a 13 mm thick end plate welded inside the brace member directly above the end supports, which locate at 100 mm from the end of the brace. The parameter ρ measures the position along the brace-to-chord intersection in the counter-clockwise direction when viewed from the right side of the specimen, as shown in Fig. 1. An angle $\rho < 180^\circ$ denotes the brace-to-chord intersection facing the observer in Fig. 1. In contrast, the angle $\rho > 180^\circ$ refers to the brace-to-chord intersection at the back of the specimen. The constant-amplitude load applies to the top of the chord member through a detachable loading fixture, creating a brace in-plane bending moment on the joint.

The experimental study performs two constant-amplitude cyclic tests on each X-joint specimen. The first test applies the cyclic brace in-plane bending to the joint until a fatigue surface crack penetrates to about 80% of the wall thickness near the bottom of the brace-to-chord intersection. The experimental procedure then rotates the specimen by 180° in plane and applies the second test with the same cyclic load. The second test shifts the fatigue cracks generated in the first test to the top of the brace-to-chord intersection, which now experiences compressive stresses. The second test terminates when a fatigue surface crack penetrates to about 80% of the wall thickness near the weld toe of the bottom brace-to-chord intersection which previously experiences compressive stresses in the first test.

The two X-joint specimens differ in the treatment on the weld surface and the weld toe. The first specimen and its flipped configuration, namely J1 and J1-F, include neither surface treatment on the weld surface, nor on the weld toe. The second specimen, denoted as J1X, has a grinded weld surface performed in an offshore fabrication yard. After the first cyclic test on the specimen J1X, the weld toes in both the brace and chord members undergo a burr grinding treatment with a radius of 3 mm, before the second cyclic test is applied to the rotated specimen J1X-F. The specimen J1X-F anticipates the longest fatigue life among all four fatigue tests and may likely incur a root crack in the PJP+ welds.

Both X-joints utilize S355 steels for the brace and the chord members. The coupon test indicates a Young's modulus of 200 GPa for the chord member and 203 GPa for the brace member. The Poisson's ratio for steels equals 0.3. The constant-amplitude load applied in all four tests has a frequency of 0.5 Hz, with a maximum load equal to 235 kN and a minimum load of 25 kN.

The boundary conditions of the joint include a roller support near the right end of the brace member and a pin-support near the left end of the brace member. The upper end of the chord has a detachable loading fixture, which transfers the load applied from a 200-ton hydraulic rig to the test specimen through the contact between the steel surfaces. The load line passes through the intersection between the centerlines of the brace and the chord, as shown in Fig. 1. The carefully designed loading fixture minimizes the un-balanced reactions at the end of the two braces, as confirmed by the experimental measurement.

2.2. Experimental results

Tab. 1 summarizes the details of the crack initiation and fatigue life for different cracks in each test. The crack initiation defined in the current study corresponds to a measured crack depth (a) of approximately 0.5 mm.

Table 1. Measured fatigue crack details in the two X-joint specimens.

Specimen	Crack	Location of crack initiation	No. of cycles		Surface roughness near the welds	
			At initiation ($a \approx 0.5$ mm)	At $a =$ 20 mm	Brace (μm)	Chord (μm)
J1	Chord crack	Left to brace-to-chord intersection ($\rho \approx 245°$)	70,000	203,000	6.2	11.2
J1-F	Brace crack B1	Left to brace-to-chord intersection ($\rho \approx 140°$)	82,000	N.A.		
	Brace crack B2	Left to brace-to-chord intersection ($\rho \approx 220°$)	106,000	N.A.		
	Chord crack	Left to brace-to-chord intersection ($\rho \approx 235°$)	26,000	159,000		
	Chord crack	Right to brace-to-chord intersection ($\rho \approx 130°$)	123,000	N.A.		
J1X	Chord crack	Left to brace-to-chord intersection ($\rho \approx 225°$)	175,000	485,000	3.5	2.5
J1X-F	Chord crack	Left to brace-to-chord intersection ($\rho \approx 225°$)	397,000	N.A.		
	Chord crack	Right to brace-to-chord intersection ($\rho \approx 225°$)	295,000	600,000		
	Brace crack	Left to brace-to-chord intersection ($\rho \approx 235°$)	525,000	N.A.		

3. NUMERICAL INVESTIGATION

The finite element models used in the current study connect a crack-front mesh generated in a specialized crack mesh generator, FEACRACK [14], with a global continuous mesh built in Patran [15] through a mesh-tieing procedure. Qian *et al.* [16-18] verified the mesh-tieing procedure for both the linear-elastic analysis and the elastic-plastic, large deformation analysis. Fig. 2 illustrates a typical half finite element model generated for the CHS X-joint. The linear-elastic analyses reported in this paper employ the finite element research code WARP3D [19], which computes the mixed mode SIF values through an interaction-integral approach. The estimation of the fatigue crack propagation life follows the Paris law,

$$\frac{da}{dN} = C\left(\Delta K_{eff}\right)^m \tag{1}$$

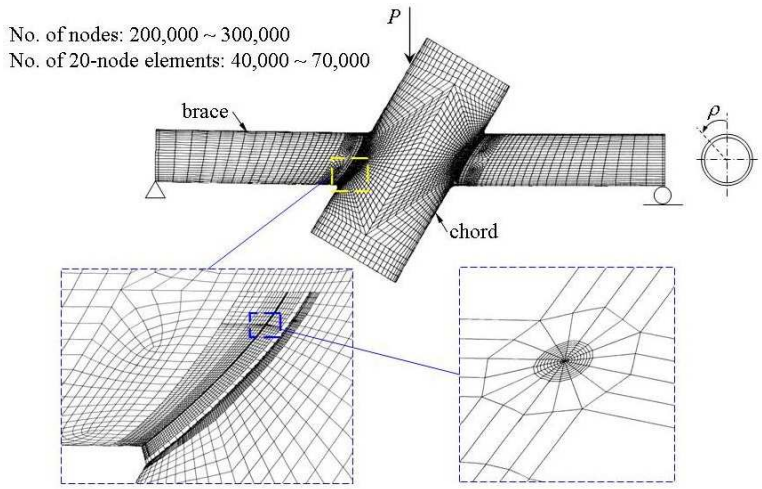

Fig. 2. A typical FE mesh for an X-joint specimen with a detailed crack-front model

where C and m refer to the material parameters obtained from the small-scale compact tension, C(T), specimens following the standard procedure outlined in ASTM E-647 [20]. The fatigue tests on the C(T) specimens, fabricated using materials from the large-scale joint specimens, yields a m value of 2.207 and a C value of 14.211×10^{-11} for ΔK measured in MPa$\sqrt{m}$ and da/dN measured in m/cycle. The effective crack driving force, ΔK_{eff} in Eq. (1), defines the range of effective stress-intensity factors calculated from the mixed-mode stress intensity factors [21],

$$K_{eff} = \left[K_I^2 + K_{II}^2 + K_{III}^2/\left(1-\upsilon\right)\right]^{0.5} \tag{2}$$

where K_I, K_{II} and K_{III} refer to the mode I, II and III stress intensity factor, respectively, and υ denotes the Poisson's ratio of the material.

3.1. Effect of crack propagation angle

Fig. 3 compares the variation of the mixed-mode SIF values with respect to the crack propagation angle at the deepest location along a semi-elliptical brace crack front and a semi-elliptical chord crack front, the locations of which correspond to the experimental observations. For the two crack depths (a/t = 0.25 and 0.5; t = thickness) considered in Fig. 3, the in-plane mode-mixity measured by the ratio K_{II}/K_I reaches zero as the crack propagates along a small positive angle, with $10^\circ < \varphi < 20^\circ$ for the brace crack and $20^\circ < \varphi < 30^\circ$ for the chord crack. This explains the reason for the fatigue crack to propagate along a positive φ angle as observed in the experiment. The effective fatigue driving force, K_{eff}, contributed mainly by the mode I SIF value, increases slightly as the angle φ increases, but shows drastic reductions as the φ angle exceeds 20° for the brace crack and 30° for the chord crack. For a typical φ angle observed in the experiment ($10^\circ < \varphi < 30^\circ$), the difference between the K_I and K_{eff} values remain within 4-10% for the brace cracks and within 3% for the chord cracks considered in Fig. 3.

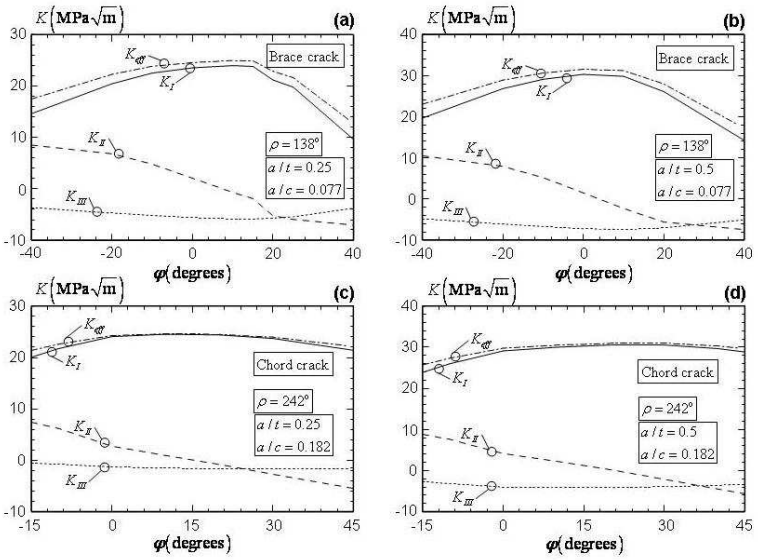

Fig. 3. Variation of the linear-elastic SIF values at the deepest crack-front location with respect to the crack propagation angle φ for: (a) a brace crack with $a/t = 0.25$ and $a/c = 0.077$; (b) a brace crack with $a/t = 0.5$ and $a/c = 0.077$; (c) a chord crack with $a/t = 0.25$ and $a/c = 0.182$; and (d) a brace crack with $a/t = 0.5$ and $a/c = 0.182$; on the left side of the X-joint

3.2. Effect of crack-front profile

The experimental investigation reveals that the crack front of a fatigue surface crack does not strictly follow a semi-elliptical shape. The current numerical study examines the effect of the crack-front shape on the computed linear-elastic stress-intensity factors, for a brace surface crack oriented at $\varphi = 15°$. Fig. 4a shows the four crack-front shapes in the numerical study: the real crack front measured from the experiment, a semi-elliptical crack, a user-defined crack front (Crack A), and a surface crack with a constant depth over more than 90% of the crack front. The real crack front in Fig. 4a refers to the brace crack B1 in the specimen J1-F (see Tab. 1). All cracks in Fig. 4a have the same crack depth ratio ($a/t = 0.8$) and the same crack aspect ratio ($a/c = 0.077$; $2c$ = crack legth) corresponding to the final crack size measured in the experiment. The "real crack" shown in Fig. 4a has a smoothened crack-front shape when built in the FE mesh generator [15] to facilitate the numerical convergence.

Figs. 4b-4d compare the mode I, II and III stress intensity factors for different crack-front shapes. The real crack shape has the smallest crack area among the four cracks considered. The small crack area for the real crack shape leads to reduced K_I values along the crack-front compared to the K_I values computed from the other three crack-front shapes. The K_I value at the deepest front location ($\rho = 138°$) in the real crack remains about 7% lower than the K_I value at the corresponding front location in a semi-elliptical crack, despite that both models contain the same maximum crack depth as shown in Fig.

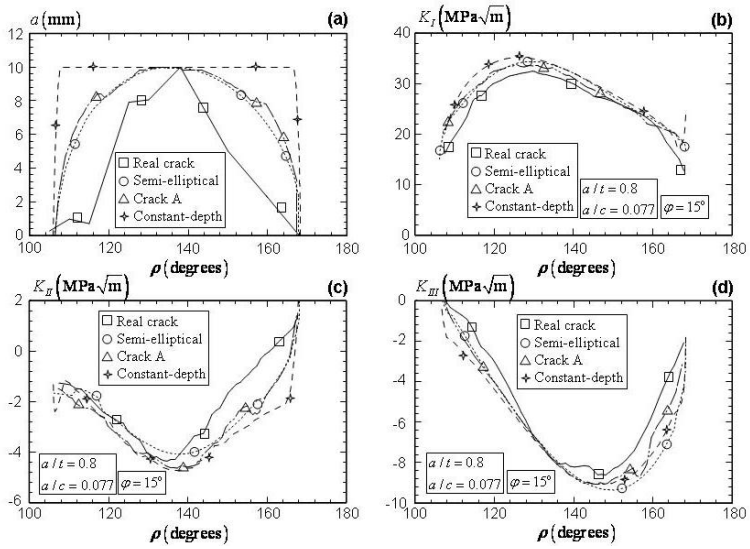

Fig. 4. (a) Different crack front profiles simulated in the FE model; (b) linear-elastic K_I values along the different crack-front profiles; (c) linear-elastic K_{II} values along the different crack-front profiles; and (d) linear-elastic K_{III} values along the different crack-front profiles

4a. The 7% difference in the stress-intensity factor, translates into a 15% difference in the crack propagation rate, using the material constants determined from C(T) specimens. Similar to the K_I value, both the mode II and mode III SIF values for the real crack shape remain small among the four crack-front shapes, as shown in Figs. 4c and 4d.

3.3. Effect of Crack Interactions

This section examines the crack interactions between the brace crack B2 (see Tab. 1) and the adjacent crack in the chord member in the specimen J1-F. Fig. 5a sketches the location of the two cracks, the crack planes of which overlap along the ρ-direction. Fig.5b shows the crack-front profiles of two sets of surface cracks measured in the experiment. As the brace crack reaches a crack depth of $a = 4$ mm, the chord crack has a crack depth of $a = 11$ mm. While the brace crack propagates to a crack depth of $a = 8.5$ mm, the crack depth in the chord reaches 20 mm. The shallow brace crack ($a = 4$ mm) overlaps with the chord crack with $a = 11$ mm from $\rho \approx 220°$ to $\rho \approx 240°$, while the deep brace crack ($a = 8.5$ mm) overlaps with the chord crack from $\rho \approx 215°$ to $\rho \approx 265°$.

The presence of the fatigue crack adjacent to the chord crack impinges on the stress field near the 3-D curved crack front and subsequently influences the magnitude of the stress-intensity factors along the crack front. The numerical procedure thus computes the SIF values along the 3-D crack front from two different FE models: the FE model with a "single" crack and the FE model with the "combined" brace crack and chord crack. Figs. 5c and 5d compare the mode I and the effective stress-intensity factors along the front of the brace crack computed from the two different finite element models. The shallow brace crack in the FE model with two cracks in Fig. 5c shows smaller SIF values over the

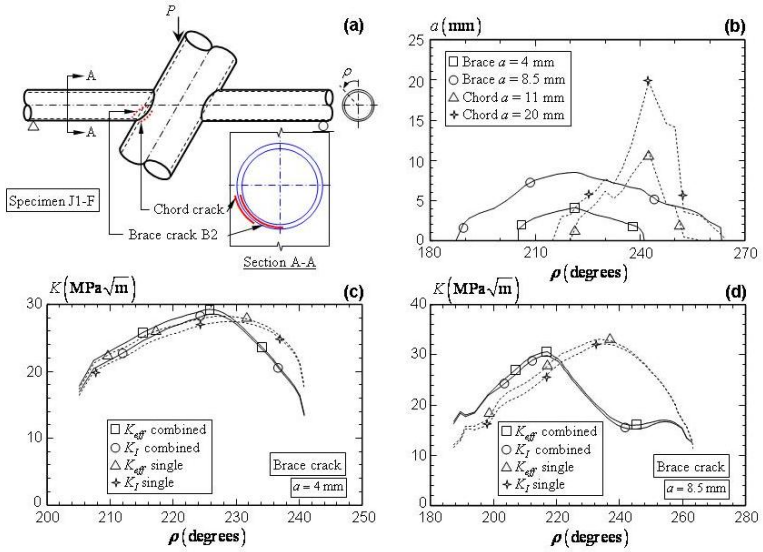

Fig. 5. (a) Location of the brace crack B2 and the chord crack in the X-joint specimen J1-F; (b) crack-front profiles for the brace and chord cracks; (c) comparison of the SIF values for the shallow brace crack; and (d) comparison of the SIF values for the deep brace crack

overlapping zone, but a slightly larger maximum SIF value than that computed from the FE model with a single brace crack. The deep crack in Fig. 5d demonstrates a pronounced effect of the interaction between the adjacent cracks in tubular joints. The presence of the chord crack reduces both the SIF values over the overlapping zone and the maximum SIF values along the crack front. The comparison between Fig. 5c and Fig. 5d indicates that the presence of adjacent crack shifts the location of the maximum SIF value as both cracks propagate. The interaction between the adjacent cracks drives a maximum crack depth at $\rho = 215°$ for the crack in the brace and at $\rho = 242°$ for the crack in the chord. The results in Figs. 5c and 5d imply that accurate estimations of the fatigue crack propagation life requires modeling of the multiple cracks in the FE model. The following section presents the estimation of the fatigue crack propagation for a brace toe crack located in the front side of the joint with $\rho < 180°$, which does not experience variations in the stress field caused by an adjacent crack, a chord toe crack in the back side of the joint ($\rho > 180°$) with the presence of an adjacent brace crack, and a weld root crack.

3.4. Estimation of Propagation Life for Toe and Root Cracks

The numerical procedure follows three steps to estimate the crack propagation life for the weld toe and root cracks in the X-joint specimen. The first step computes the linear-elastic SIF values at the deepest crack-front location based on the measured crack-front profiles and the crack propagation angles of $\varphi = 15°$ for the brace crack and $\varphi = 20°$ for the chord crack. With the SIF values computed, the second step calculates the number of cycles required to propagate a unit crack depth, or dN/da based on Eq. (1). The third step

then performs a polynomial fit of the dN/da data, which enables a closed-form integration of the number of cycles required to propagate the fatigue crack from a small crack depth to the final crack depth.

Figs. 6a and 6b compare the estimated fatigue life using the above procedure with the experimental observations for the deepest crack-front location ($\rho = 138°$) in the brace crack B1 and for the deepest crack-front location ($\rho = 242°$) in the chord in the specimen J1-F. The chord crack in J1-F locates at the back side of the joint, with an adjacent crack near the weld toe in the left brace. The SIF values used to estimate the chord crack propagation, therefore, computes from FE models with both cracks. The close agreement between the experimental data and the numerical prediction in Figs. 6a and 6b validates the current procedure to estimate the crack propagation based on Eq. (1).

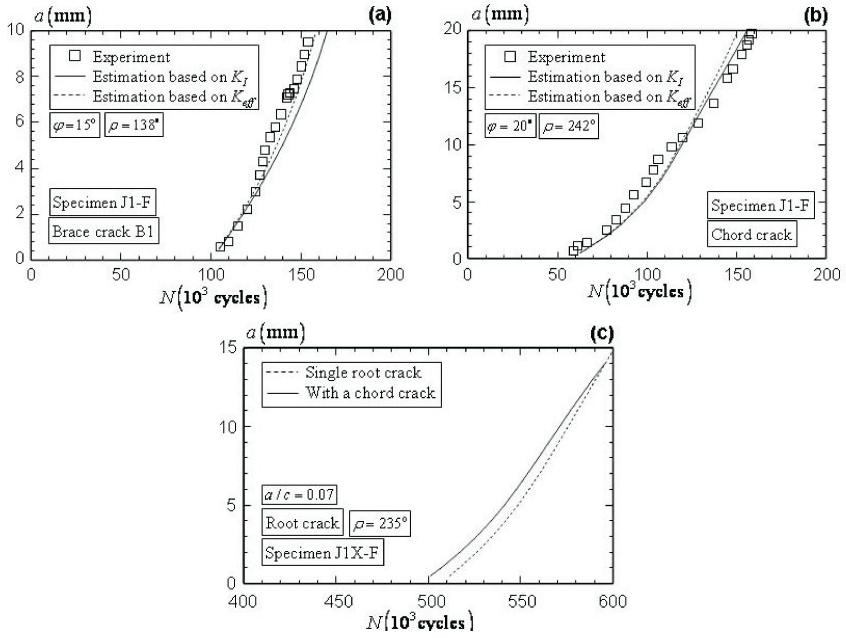

Fig. 6. Comparison between the estimated fatigue crack propagation and the test record for (a) the brace crack B1 in J1-F; (b) the chord crack in J1-F; and (c) the estimated fatigue crack propagation for the root crack in J1X-F

Monitoring the initiation and propagation of the fatigue crack at the root of the welds remain a challenging task in today's engineering laboratories. Fig. 6c extends the same procedure to estimate the propagation life for the root crack observed in the specimen J1X-F, with the objective to estimate the initiation of the root crack. The numerical procedure assumes a semi-elliptical shape of the root surface crack perpendicular to the outer surface of the chord, with the crack aspect ratio fixed at $a/c = 0.07$. This crack aspect ratio estimates from the final root crack measured by the post-test sectioning. The SIF values computed for the root crack includes the presence of an adjacent toe crack in the chord material. Fig. 6c shows that the initiation of the root crack occurs approximately

at 500,000 cycles. This estimation complies with the fact that root cracking does not take place after 485,000 cycles in the specimen J1X based on the post-test sectioning observations.

4. SUMMARY AND CONCLUSIONS

This study examines the fatigue performance of the tubular joints fabricated using the enhanced partial joint penetration welds, through four constant-amplitude tests on two large-scale CHS X-joint specimens. The numerical study examines a few important, commonly observed aspects on the fatigue crack propagation in circular hollow section joints, including the effect of the crack propagation angle, the effect of the crack-front profile, and the interaction between adjacent fatigue cracks. The present study supports the following observations and conclusions:

- Many assumptions in the conventional approach to estimate the surface crack propagation in large-scale 3-D structures, for example, the direction of the fatigue crack propagation and the semi-elliptical shape of the fatigue surface crack, may lead to incorrect estimations of the stress-intensity factors along the crack front and subsequently incorrect predictions of the real fatigue crack life. For the X-joint specimens investigated in the current study, the surface crack tends to propagate in a direction oriented towards the welds with $10^\circ \leq \varphi \leq 20^\circ$, over which the mode II loading approaches zero. The semi-elliptical crack-front shape, commonly assumed for fatigue crack propagations 3-D structures/specimens, leads to a slightly higher (about 7%) mode I SIF values than that computed from the real crack-front shape for the X-joint specimen reported in this study. Coupled with a Paris exponent of $m = 2$ to 5, this leads to an over-estimation in the fatigue crack propagation rate of 14% to 40%.

- Initiations and propagations of multiple fatigue cracks with overlapping crack planes delays the fatigue crack propagations, by reducing the SIF values along the overlapping zone. This interaction delays the fatigue crack propagations in the grinded specimens J1X and J1X-F, which evolve multiple crack propagations along the brace-to-chord intersection.

ACKNOWLEDGEMENT

The financial supports provided by the McDermott International Inc., Nippon Steel Engineering Co. and American Bureau of Shipping are gratefully acknowledged. The authors would also like to extend their gratitude to the research scholarship offered by the National University of Singapore.

REFERENCES

[1] American Welding Society (AWS), Structural welding code – steel. AWS D1.1/D1.1 M:2008, 21^{st} Ed, (2008).

[2] X. Qian, P.W. Marshall, W.K.D. Cheong, Y. Petchdeman, Z. Chen, Partial joint penetration plus welds for tubular joints: fabrication and SCFs, *Weld. World,* 53, (2009), 143-148.

[3] American Petroleum Institute (API), Recommended Practice for Ultrasonic and Magnetic Examination of Offshore Structural Fabrication and Guidelines for Qualification of Technicians. 4^{th} Ed, API RP 2X, (2004).

[4] A. Hobbacher, (Ed.), Recommendations for Fatigue Design of Welded Joints and Components. IIW Doc XIII-2151r1-07/XV-1254r1-07. International Institute of Welding, (2007).
[5] American Petroleum Institute (API), Recommended Practice for Planning, Designing and Constructing Fixed Offshore Platforms, 21^{st} Ed, API RP 2A WSD, (2000).
[6] W. Fricke, Fatigue analysis of welded joints: state of development, *Mar. Struct.*,16 ,(2003), p185.
[7] E.C. Rodabaugh, Review of data relevant to the design of tubular joints for use in fixed offshore platforms, *WRC Bulletin*, 256, (1980).
[8] Failure Control Ltd, MaTSU, Background to new fatigue guidance for steel joints and connections in offshore structures. Health and Safety Executive, Offshore Technology Report, OTH 92 390, (1999).
[9] A. Schumacher, A. Nussbaumer, Experimental study on the fatigue behavior of welded tubular K-joints for bridges, *Eng. Struct.*, 28, (2006), 745-755.
[10] T. Iwasaki, M. Kawahara, K. Asano, Fatigue crack growth behavior in welded tubular joints in T, TY and K, in: *Offshore Technology Conf.*, 30 April – 7 May 1979, Texas, USA. 3423-MS.
[11] D.R.V. Van Delft, C. Noordhoek, J. De Back, Evaluation of the European fatigue test data on large-size welded tubular joints for offshore structures, in: *Offshore Technology Conf.*, 6-9 May, 1985, Texas, USA, 4999-MS, (1985).
[12] C.H. Jo, S.W. Im, W.C. Cho, K.K. Park, Fatigue crack in large-scale tubular joints for offshore structures, *Sci. China Tech. Sci.*, 54, (2011), 705-714.
[13] MSL Engineering Ltd., Fatigue life implications for design and inspection for single sided welds at tubular joints. Offshore Technology Report, OTO 1999 022, Health and Safety Executive, (1999).
[14] Quest Integrity Group, FEA Crack 3D Finite Element Software for Cracks Version 3.2 User's Manual. Quest Integrity Group, United States, 2010.
[15] X.D. Qian, A. Romaijin, J. Wardenier, Y.S. Choo, Y. S. An automatic FE mesh generator for CHS tubular joints, in: *Proc.* 12^{th} *Int. Offshore Polar Engineering Conf.*, ISOPE, Kitakyushu, Japan, Vol 4, (2002), pp. 1-8.
[16] X. Qian, R.H.Jr. Dodds, Y.S. Choo, Mode mixity for circular hollow section X-joints with weld toe cracks, *J. Offshore Mech. Arct.*, 137, (2005), 269-280.
[17] X. Qian, Stress-intensity factors for circular hollow section V-joints with a rack-plate chord, *Fatigue Fract. Eng. M.*, **32**(1), (2009), 61-79.
[18] X. Qian, R.H.Jr. Dodds, Y.S Choo, Elastic-plastic crack driving force for tubular X-joints with mismatched welds, *Eng. Struct.*, 27, (2005), 1419-1434.
[19] B. Healy, A. Gullerud, K. Koppenhoefer, A. Roy, S. RoyChodhury, M. Walters, B. Bichon, K. Cochran, A. Carlyle, R.H. Dodds. WARP3D-Relese 16.3.1 3-D dynamic nonlinear fracture analyses of solids using parallel computers. Structural research series no. 607. University of Illinois at Urbana Champaign. (2010).
[20] American Society of Testing and Materials (ASTM), E-647, Standard Test Method for Measurement of Fatigue Crack Growth Rates. ASTM International. United States, (2008).
[21] R.H. Chong, S. Han, S., G.S. Gipson, Reliability of solution method and empirical formulas of stress intensity factors for weld toe cracks of tubular joints, in: *Proc.* 10^{th} *Offshore Mechanics and Arctic Engineering Conf.*, ASME, 3-B, (1991), 441-452.

Received January 02, 2012

VIETNAM ACADEMY OF SCIENCE AND TECHNOLOGY
VIETNAM JOURNAL OF MECHANICS VOLUME 35, N. 1, 2013

CONTENTS